Photocatalysis

https://www.sciltp.com/journals/photocatalysis

Supplementary Information

Low-Temperature Photo-Thermal Synthesis of Ammonia over K-Promoted Ru/CeO_2 Catalyst

Angel Sousa, Alejandra Rendón-Patiño, Xinhuilan Wang, Diego Mateo * and Jorge Gascon *

Advanced Catalytic Materials (ACM), KAUST Catalysis Center (KCC), King Abdullah University of Science and Technology (KAUST), Thuwal 23955-6900, Saudi Arabia

* Correspondence: diego.mateo@kaust.edu.sa (D.M.); jorge.gascon@kaust.edu.sa (J.G.)

Table of contents

1 Experimental section

1.1 Materials and reagents

Cerium (IV) oxide nanopowder (< 50 nm particle size), titanium (III) oxide, and potassium carbonate were purchased from Sigma Aldrich. Ruthenium (III) chloride hydrate was purchased from Alfa Aesar. All materials were used without further purification. Deionized water was obtained with a Milli-Q® system (18.2 MΩ·cm).

1.2 Catalyst preparation

For the K-promoted Ru(x)CeO_2 catalyst preparation, a certain amount of ruthenium (III) chloride and potassium carbonate was weighted to achieve the desired Ru and K loading. Both precursors were transferred into a vial and subsequently dissolved in 40 drops of Milli-Q® water using ultrasounds for 15 minutes. Once the solids were dissolved, we impregnated 500 mg of cerium oxide with the solution using a glass pipette, drop by drop. No treatment of CeO_2 preceded the wet impregnation. This process was intercalated with 5 minutes drying intervals to evaporate the excess of liquid and promote a homogenous impregnation of the sample.

The following steps consisted of the calcination and reduction of the resulting material. The calcination was performed at 400 °C for 2 h with a heating rate of 5 °C min^{-1} in air. Subsequently, the sample underwent a reduction step at 350 ºC for 2 h with a heating rate of 5 ºC min^{-1} in a gas mixture consisting of ~ 6% Hydrogen (H_2) in Argon (Ar) at 80 mL min^{-1}. After cooldown to room temperature, the material underwent a passivation for 1 h with a gas mixture consisting of ~5% Oxygen (O_2) in Nitrogen (N_2) at 20 mL min^{-1} to obtain the K-promoted Ru/CeO_2 catalyst.

For the CeO_2 and K-promoted CeO_2 samples measured in PXRD, Raman and EPR, the same procedure was followed without the addition of the Ru precursor.

1.3 Characterization

Powder X-ray Diffraction (PXRD)

XRD analysis was carried out using a Bruker D8 Advanced diffractometer in Bragg-Brentano geometry using a Copper tube operating at 40 kV and 40mA. Diffractograms were measured over the 2θ range of 10-90° using a step-size of 0.018° with a dwell time per step of 5 seconds.

Temperature Programmed Reduction (TPR)

TPR measurements were performed on a Micromeritics Autochem 2920 instrument. The sample underwent a drying process prior to the measurement. A mixture of H_2 (10%) in Ar was introduced in the reactor with a flow of 20 $mL \cdot min^{-1}$. The temperature of the samples was increased linearly at a heating rate of 10 $ºC \cdot min^{-1}$ and the hydrogen consumption was monitored using a TCD for signal acquisition.

Inductively Coupled Plasma Optical Emission Spectrometry (ICP-OES)

Standard with four different concentrations (1 ppm, 10 ppm, 25 ppm, and 100 ppm) were prepared by diluting a 1000 ppm standard stock solution.

Each $Ru(x)CeO_2$ sample was transferred to a Teflon tube and mixed with an acid solution (6 mL concentrated HCL, 2 mL concentrated HNO_3, and 1 mL HF). The materials (acid mixture and sample) were digested using an ultra-wave digester (milestone ultra-wave microwave digester). The digested samples were diluted with water and subjected to Inductively Coupled Plasma Optical Emission Spectrometry (ICP-OES) testing. The sample concentrations were measured with an Agilent ICP-OES 5110 equipment.

Raman Spectroscopy

Room temperature Raman spectra were acquired by using a confocal Raman Microscope WITec Apyron. The wavelength of the applied exciting laser was 532 nm, and a Zeiss LD EC Epiplan-Neofluar Dic 50x / NA 0.55 objective lens was used to focus. A laser power of 5 mW, an integration time of 5 s, an accumulation number of 10 and a grating of 300 g/mm were set for all acquisitions to collect the Raman spectra.

Photoluminescence (PL)

Photoluminescence measurements were carried out on a Fluorescence spectrometer Agilent-Varian (AA280FS/Carry Eclipse) using an excitation wavelength of 374 nm.

Transient Photocurrent measurements

Transient photocurrent measurements were carried out using an SP-150 potentiostat (Bio-Logic) in a three-electrode system with a 1 M KCl aqueous solution. The working electrode consisted of FTO glass coated with a catalyst dispersion, the counter electrode was platinum foil, and the reference electrode was a saturated Ag/AgCl electrode. To prepare the working electrode, 80 µL of a catalyst dispersion (10 mg of catalyst, 20 µL of 1 wt.% Paraloid acetone solution, and 200 µL of ethanol) were applied to the FTO surface, covering an area of 1.0 x 1.0 cm^2.

In situ Diffuse reflectance infrared Fourier transform spectroscopy (DRIFTS)

In situ DRIFTS spectra were registered using a Thermo Scientific Nicolet 6700 series Fourier transform infrared (FT-IR) spectrometer equipped with a Harrick Praying Mantis High Temperature reaction chamber. Powder samples were placed into the sample cup and packed. A mixture of H_2 and N_2 (3:1 ratio) was introduced in the cell at a flow of 10 $mL \cdot min^{-1}$. Once the reaction chamber was purged, it was pressurized to 10 bar. A temperature of 350 °C was maintained during all the experiments. DRIFT spectra were recorded every 2 minutes during a total reaction time of 120 minutes. For the experiments under irradiation, a white LED source (UHP-T-WCS-DI, Prizmatrix) was introduced into the chamber during DRIFTS measurements.

High-Resolution Transmission Electron Microscopy (HR-TEM)

Transmission electron microscopy (TEM) images were acquired using a Titan ST microscope and a Titan Cs-probe corrected microscope (FEI Company, USA) at 300 keV. All samples were prepared dry and placed onto copper grids coated with carbon film (300 mesh).

Scanning transmission electron microscopy with high-angle annular dark-field (STEM-HAADF)

Scanning transmission electron microscopy with high-angle annular dark-field (STEM-HAADF) images were acquired using the Titan Cs-probe corrected microscope (FEI Company, USA) at 300 kV. The STEM-HAADF data were collected with a convergence angle of 17 mrad and an inner

HAADF angle of 49 mrad. Image sizes were set to 2048 × 2048 pixels with a dwell time of 8 µs. Additionally, composition mapping was generated using Energy-Dispersive X-ray Spectroscopy (EDXS) elemental distributions. These images were configured to 512 × 512 pixels with a 20 µs dwell time and 100 frames. The resulting elemental maps for Ru, O, Ce, and K were filtered with a Gaussian filter ($\sigma = 0.7$) based on net intensities, which were corrected for background and fitted.

X-Ray Photoelectron Spectroscopy (XPS)

X-ray photoelectron spectroscopy measurements were performed on a K-Alpha spectrophotometer (Thermo-Scientific) with a high-resolution monochromator. All spectra were measured using monochromatized Mg-K_α radiation by a double crystal monochromator with the hemispherical analyzer. The binding energies were calibrated using the 1 s transition of carbon (C1s, 284.60 eV).

UV-vis diffuse-reflectance spectroscopy

Diffuse reflectance spectra were collected with a JASCO V-670 spectrophotometer with an integrating sphere in the acquisition range of 300-800 nm. Barium sulfate ($BaSO_4$) (Sigma, 99% purity) was used as a background standard.

Ammonia Temperature-programmed Desorption (NH_3-TPD)

The NH_3 temperature-programmed desorption (NH_3-TPD) analyses were performed using a Harrick Praying Mantis High-Temperature reaction chamber. The 150 mg sample was initially reduced at 200 °C for 120 minutes under 6 vol% H_2/Ar flow. After cooling down, the sample was flushed with argon for 30 minutes. Subsequently, the sample was exposed to a flow of 50 vol% NH_3/Ar for 60 minutes and then flushed with argon for 30 minutes at 50 °C to remove the physical adsorbed NH_3. Then NH_3-TPD measurement was performed by recording the corresponding gas phase evolution via INFICON Transpector CPM100 mass spectrometry (MS) while heating the catalyst from 50 °C to 600 °C at a rate of 5 °C min^{-1} under an argon flow. To investigate the effect of illumination on NH_3 decomposition, light was introduced into the reaction chamber during the NH_3 desorption using a white LED source (UHP-T-WCS-DI, Prizmatrix).

Electron paramagnetic resonance (EPR)

All Electron paramagnetic resonance (EPR) spectra were measured using a Bruker ELEXSYS E500 X-band spectrometer operating in continuous wave (CW) mode. The system was configured

with a super-high Q cavity (model ER 4122 SHQ) to enhance sensitivity and resolution. To produce comparable data, all measurements were conducted under the same instrumental parameters and conditions at ambient temperature.

The microwave frequency was stabilized at approximately 9.867 GHz, with power attenuation set to 25 dB, corresponding to an output power of 0.4743 milliwatts. A field modulation amplitude of 5 Gauss and a modulation frequency of 100 kHz were applied consistently throughout the experiment. Spectral acquisition and signal processing were performed using Bruker Xenon software (Bruker BioSpin, Rheinstetten, Germany).

2 Catalytic Tests

Photo-thermal ammonia synthesis

For the photo-thermal catalytic testing, 30 mg of K-promoted $RuCeO_2$ was loaded into the Harrick reaction chamber (HVC-MRA-5). A 300 W Xe lamp was used as irradiation source. The temperature readings were registered by two thermocouples: one located below the catalytic bed, and another placed below its surface (<1 mm) to avoid direct light illumination of the thermocouple tip. A heating cartridge provided external heating to the catalyst bed. Typically, hydrogen (H_2) and nitrogen (N_2) were introduced inside the reaction chamber with a total flow of 10 $mL \cdot min^{-1}$ in a 3:1 ratio, accounting for a GSHV of 20000 $mL \cdot g^{-1} \cdot h^{-1}$. After purging for 15 minutes, the ammonia synthesis reaction was carried out at 350 °C and different pressures ranging from 5 to 20 bar. In the case of the dark experiments with indirect illumination, an additional thin layer of 30 mg of Ti_2O_3 was deposited on top of the catalyst and the reaction was carried out under similar conditions.

3 Supporting Images

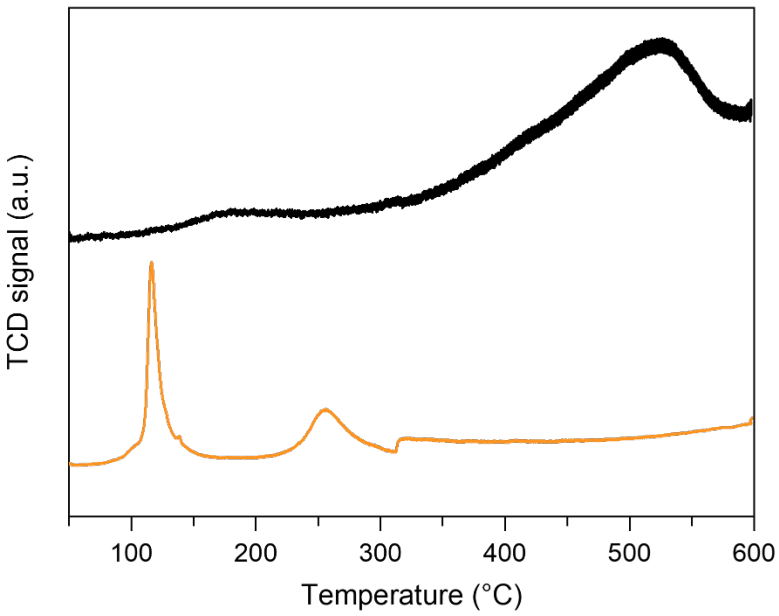

Figure S1. Temperature programmed reduction (TPR) of pristine CeO_2 (black) and K-promoted Ru(2)/CeO_2 (orange) samples.

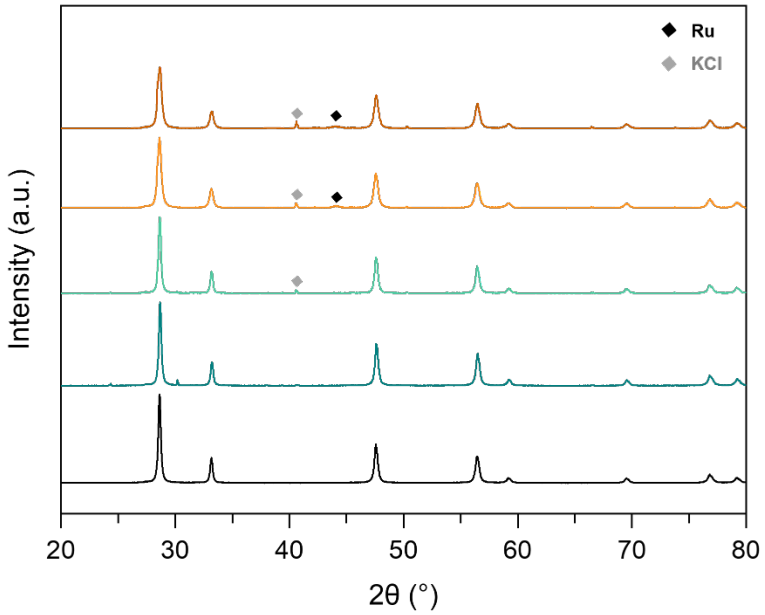

Figure S2. PXRD patterns of pristine CeO_2 and K-promoted Ru(*x*)/CeO_2 samples, where *x* stands for the Ru wt.% content, from 1 to 4 wt.% (pristine CeO_2 – black, 1 – dark green, 2 – green, 3 – orange, and 4 – brown).

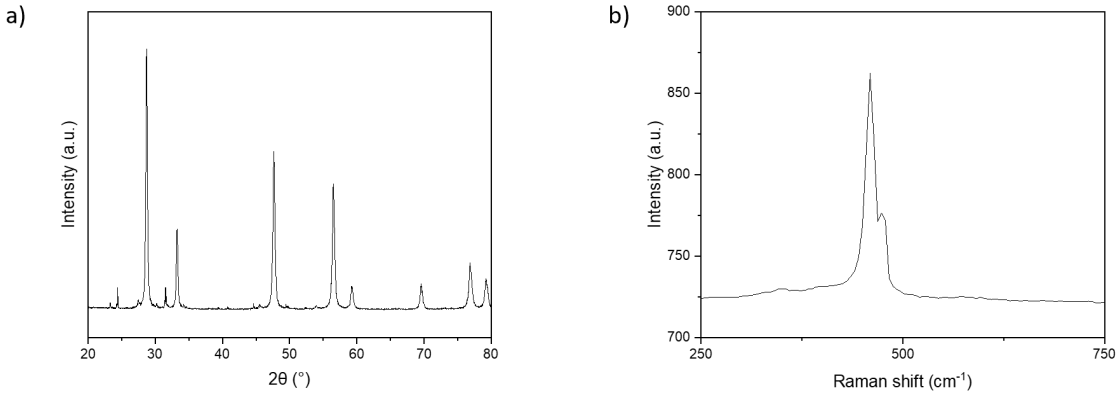

Figure S3. a) PXRD diffractogram and b) Raman spectrum measured for the K-promoted CeO_2 sample.

Table S1. ICP-OES values for the K-promoted Ru(*x*)/CeO_2 samples.

Sample	Ru content (wt. %)
Ru(1)/CeO_2	0.87 ± 0.01
Ru(2)/CeO_2	2.20 ± 0.03
Ru(3)/CeO_2	3.43 ± 0.06
Ru(4)/CeO_2	4.30 ± 0.07

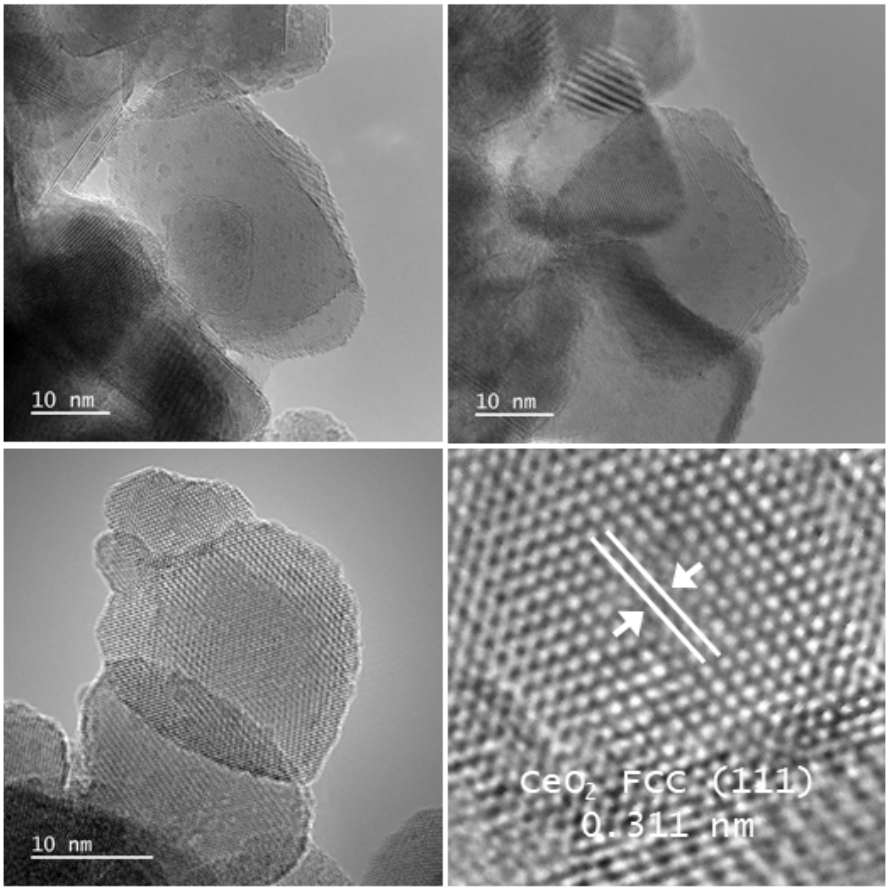

Figure S4. HR-TEM images of K-promoted Ru(3)/CeO_2.

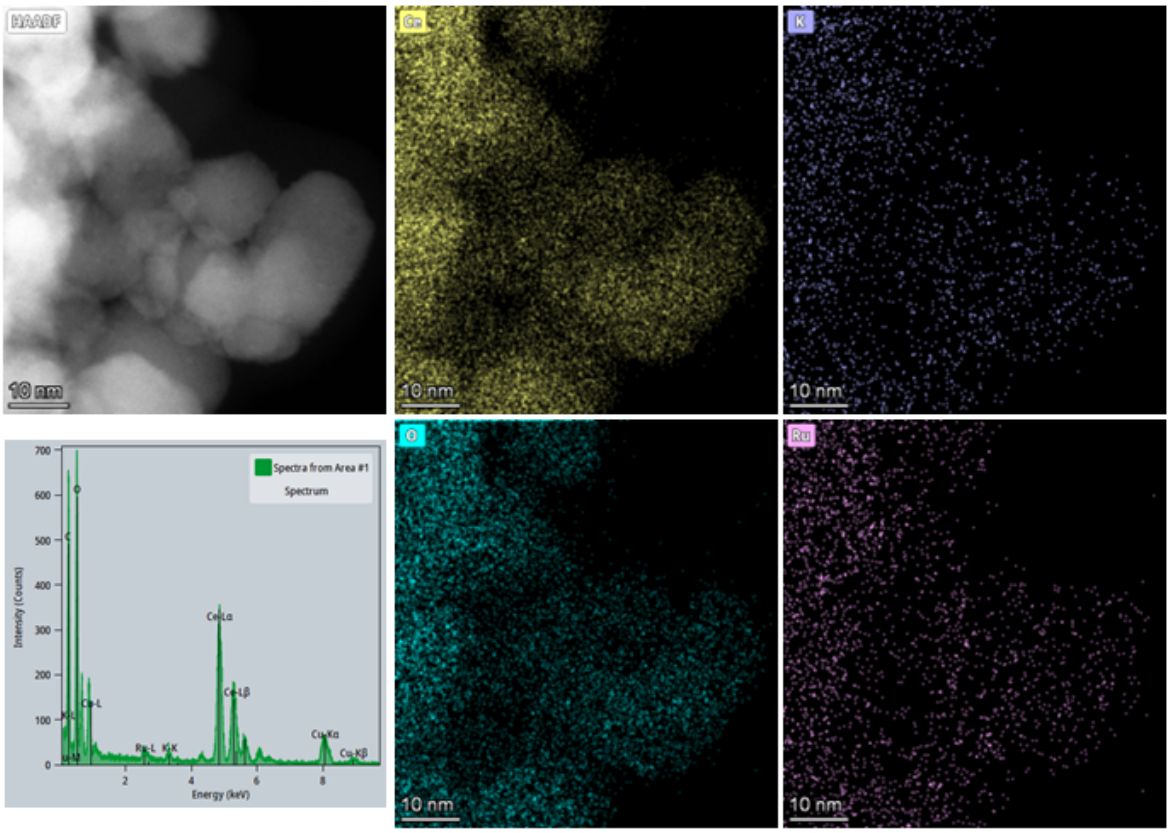

Figure S5. HAADF-STEM images together with elemental mappings by EDX analysis showing the presence of cerium (yellow), potassium (purple), oxygen (turquoise) and ruthenium (pink) in the K-promoted Ru(3)/CeO_2 sample.

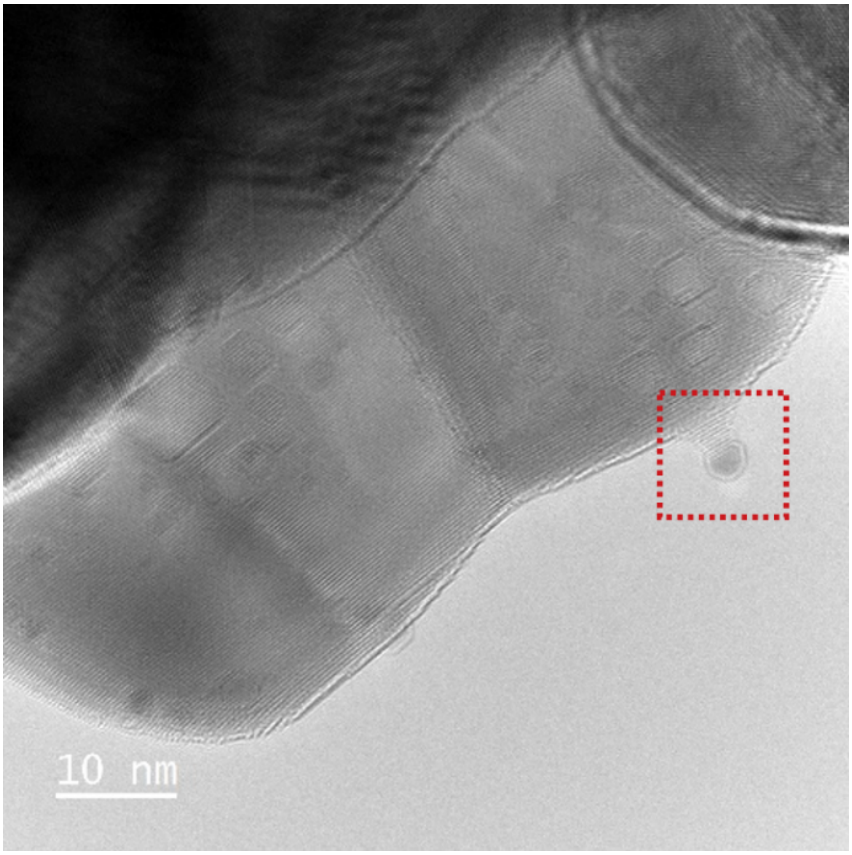

Figure S6. HR-TEM image of Ru particle encapsulation by the CeO_2 support.

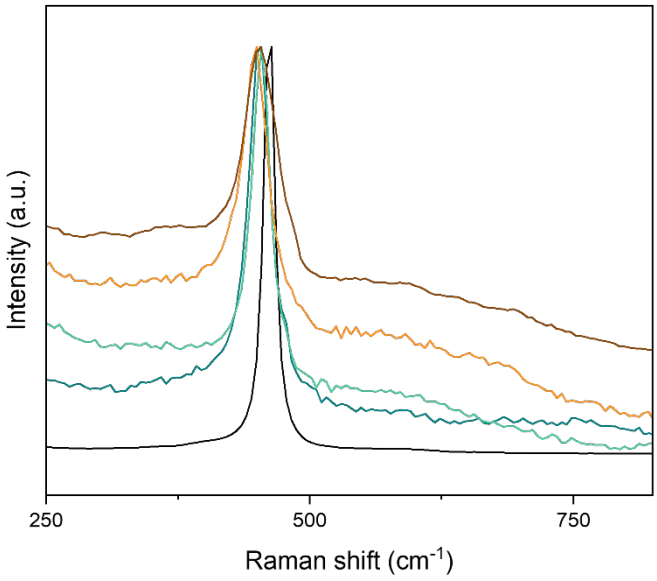

Figure S7. Raman spectra of pristine CeO_2 and K-promoted Ru(*x*)/CeO_2 samples, where *x* stands for the Ru wt.% content, from 1 to 4 wt.% (pristine CeO_2 – black, 1 – dark green, 2 – green, 3 – orange, and 4 – brown) measured under N_2 atmosphere.

Table S2. Ratio between the D and F_{2g} peak intensities calculated for pristine CeO_2 and K-promoted Ru(*x*)/CeO_2 samples, where *x* stands for the Ru wt.% content, from 1 to 4 wt.%.

Sample	$\frac{I_{600}}{I_{462}}$
CeO_2	0.01
Ru(1)/CeO_2	0.09
Ru(2)/CeO_2	0.13
Ru(3)/CeO_2	0.28
Ru(4)/CeO_2	0.32

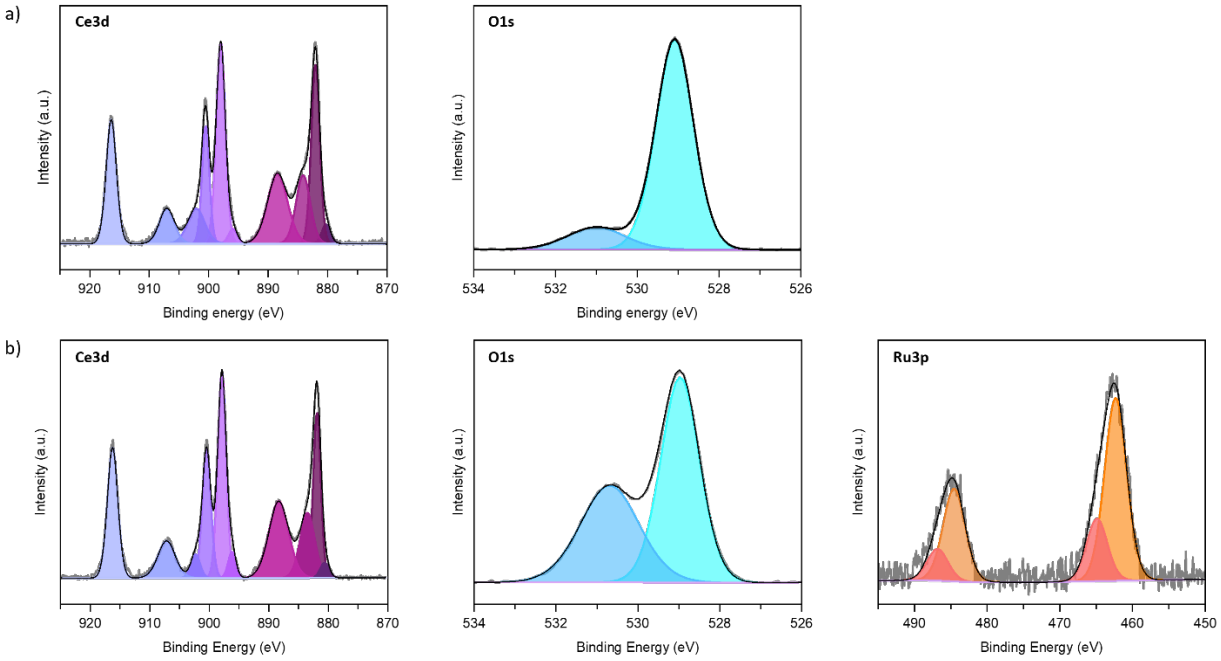

Figure S8. XPS spectra of a) pristine CeO_2 and b) K-promoted Ru(3)/CeO_2 samples.

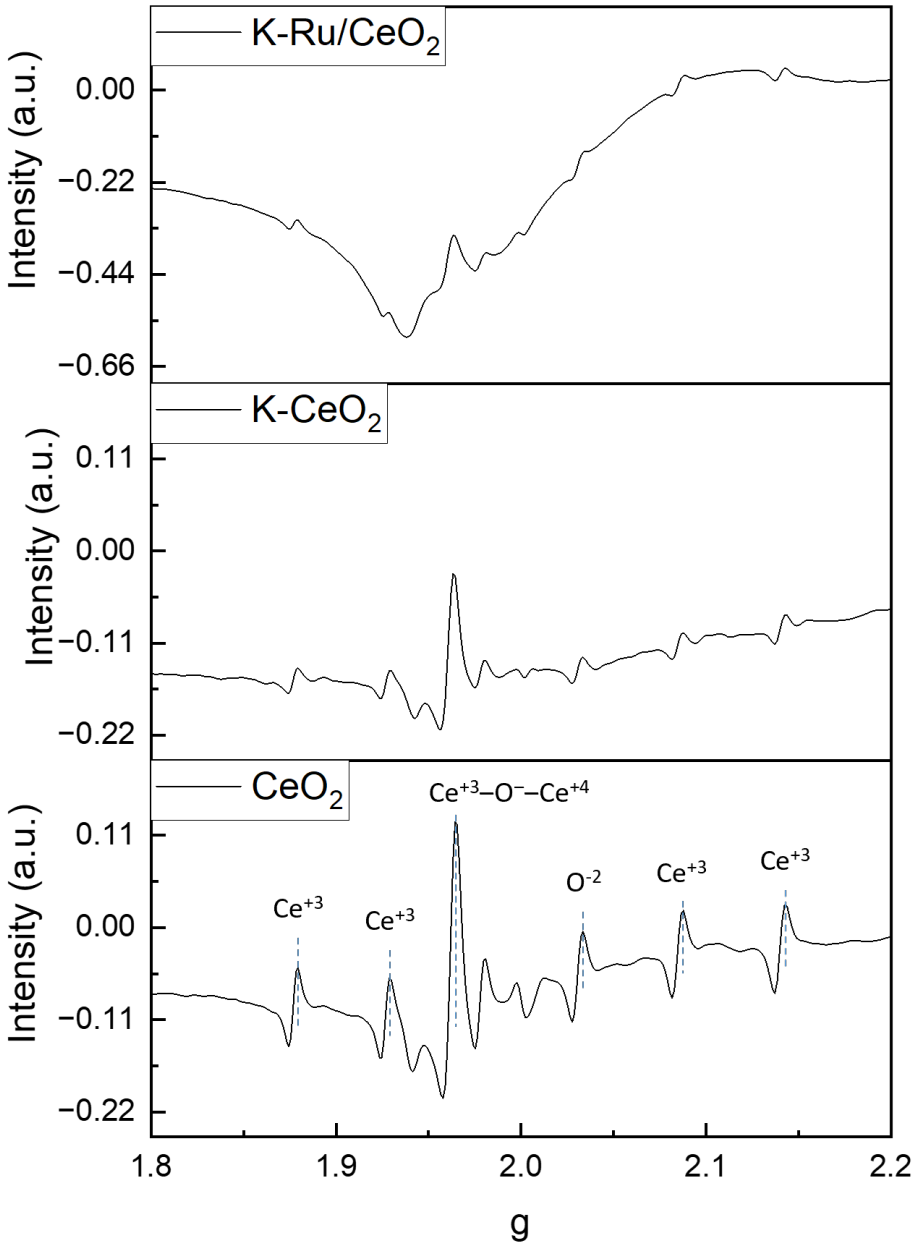

Figure S9. EPR measurements of CeO_2, K-promoted CeO_2 and K-promoted Ru(3)/CeO_2.

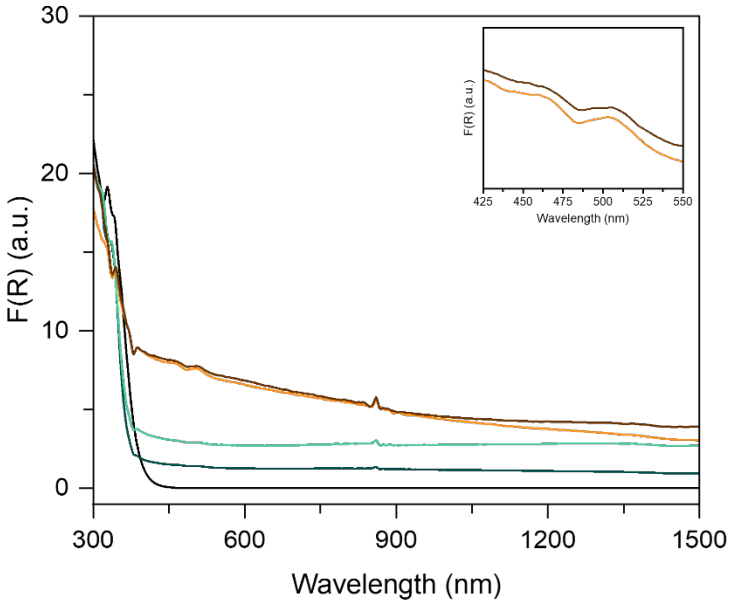

Figure S10. UV-vis-NIR diffuse reflectance spectra of pristine CeO_2 and K-promoted Ru(*x*)/CeO_2 samples, where *x* stands for the Ru wt.% content, from 1 to 4 wt.% (pristine CeO_2 – black, 1 – dark green, 2 – green, 3 – orange, and 4 – brown).

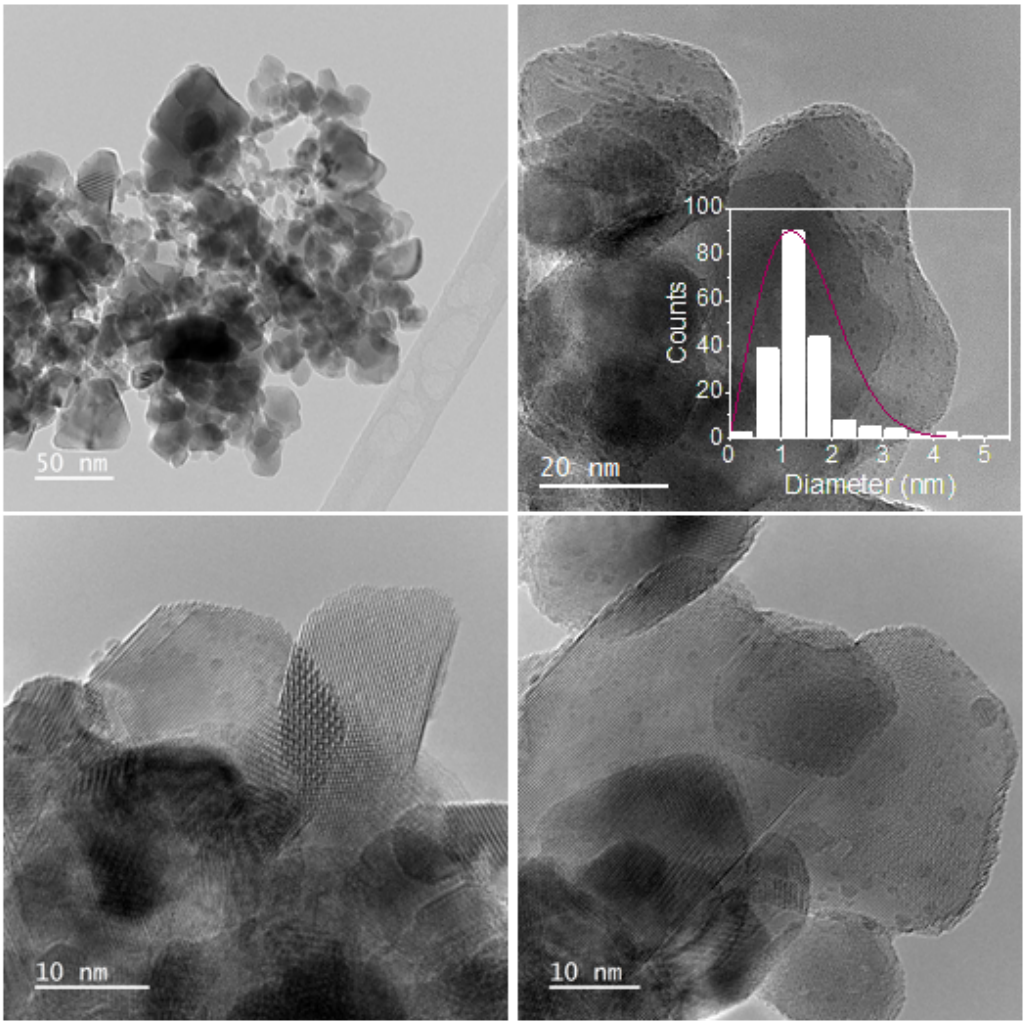

Figure S11. HR-TEM images of K-promoted Ru(4)/CeO_2 together with the particle size distribution (inset).

Table S3. Summary of the state-of-the-art catalysts for the photo-thermal NH_3 synthesis.

Catalyst	Metal Loading (wt.%)	Reaction Conditions	Production rate ($\mu mol\ g^{-1}\ h^{-1}$)	Reference
$Cs(6)Ru(6)@ZrO_2$	2.0	350 °C 0.1 Mpa Xe lamp	5100	[1]
Cs-Ru@ST	2.0	350 °C 0.1 Mpa Xe lamp	3600	[2]
Cs-Ru/MgO	2.5	333 °C 0.1 Mpa Blue LED	4464	[3]
α-Fe	100.0	0.1 Mpa Xe lamp	2538	[4]
Co@C-ZIF-67	36.0	450 °C 2 MPa Xe lamp	8000	[5]
Ru/C	3.6	380 °C 0.1 MPa Sunlight	3500	[6]
Pt-Ptn-TiN	–	280 °C 0.1 MPa Xe lamp	500	[7]
Ru/TiO_2	4.0	350 °C 1 MPa Xe lamp	240	[8]
$Ru(3)/CeO_2$	3.4	350 °C 2 Mpa Xe lamp	19700	***This work***

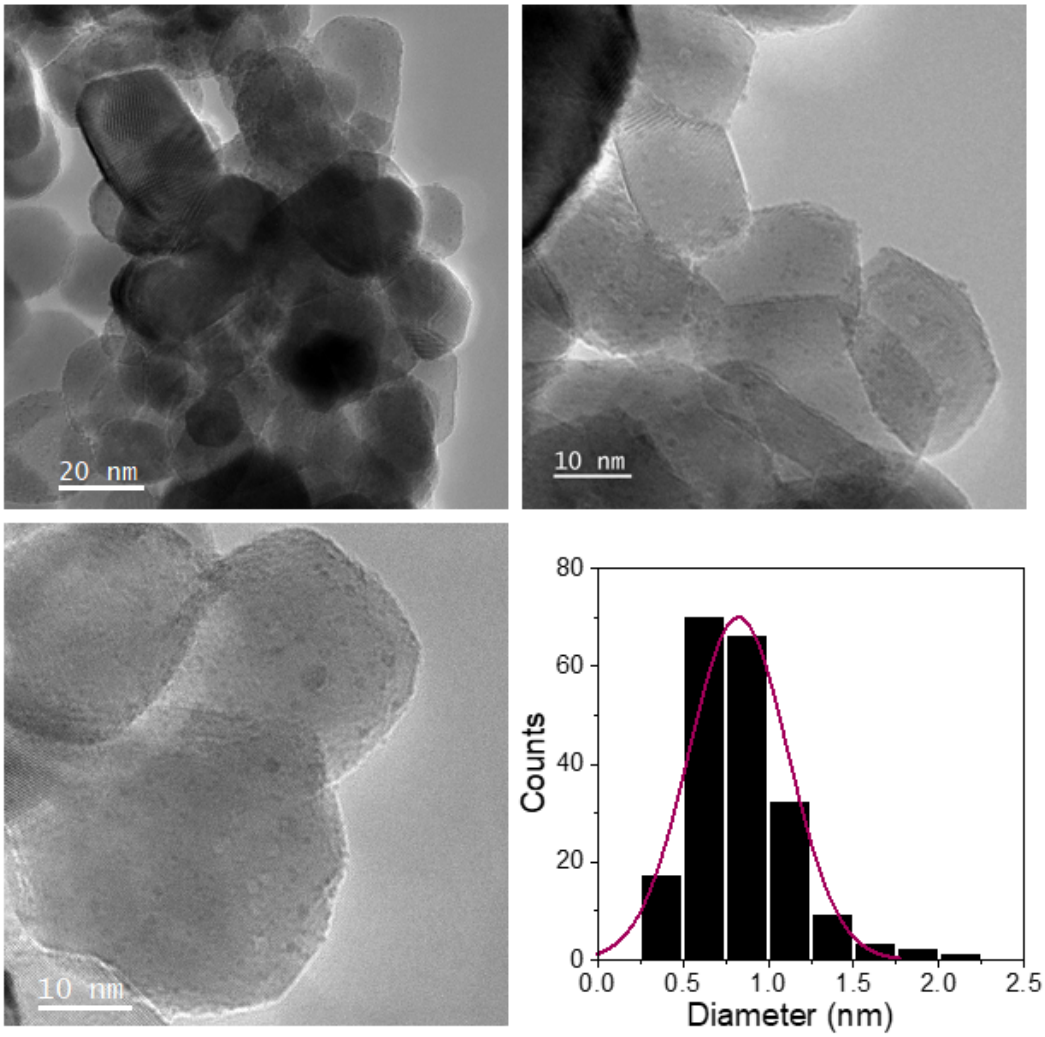

Figure S12. HR-TEM images of spent K-promoted Ru(3)/CeO_2 together with the particle size distribution.

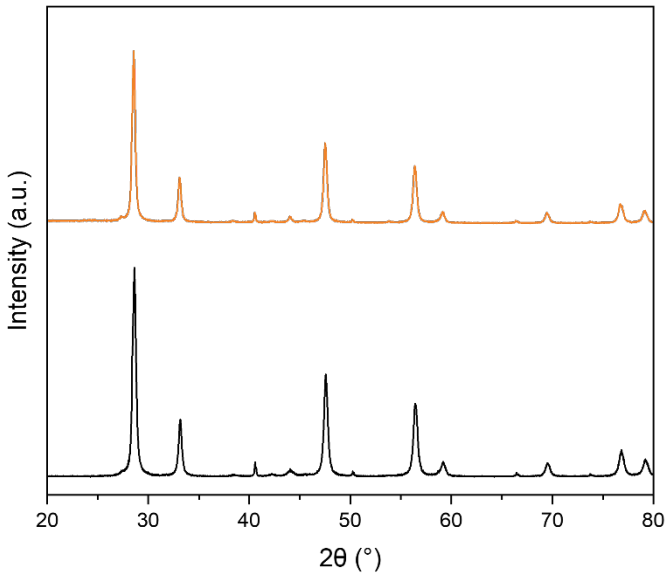

Figure S13. PXRD of fresh (black) and spent (orange) K-promoted Ru(3)/CeO_2.

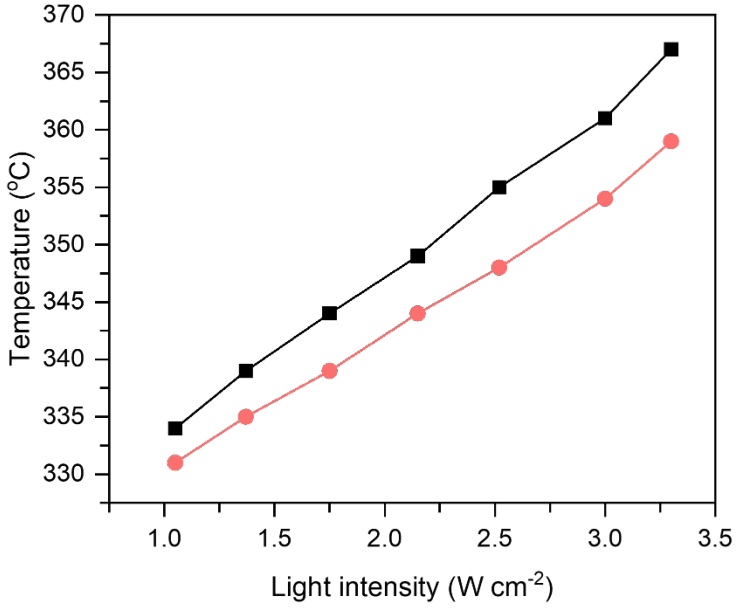

Figure S14. Temperature displayed by the catalyst under direct (salmon) and indirect (black) illumination at different light intensities.

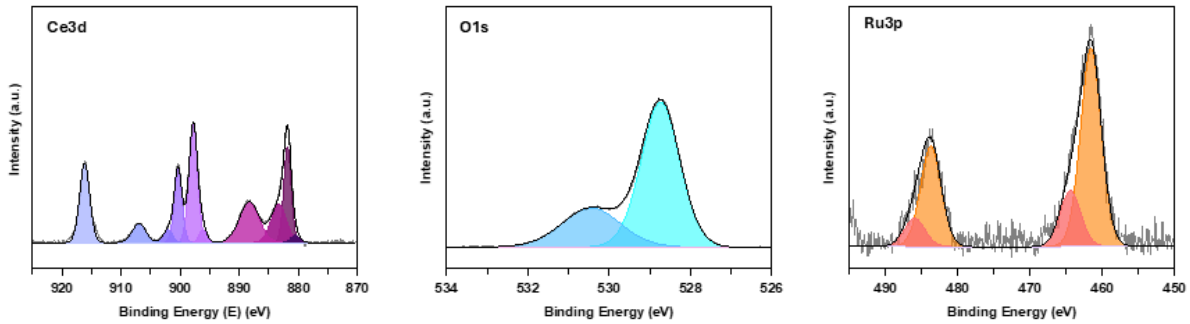

Figure S15. XPS spectra of spent K-promoted Ru(3)/CeO_2 sample.

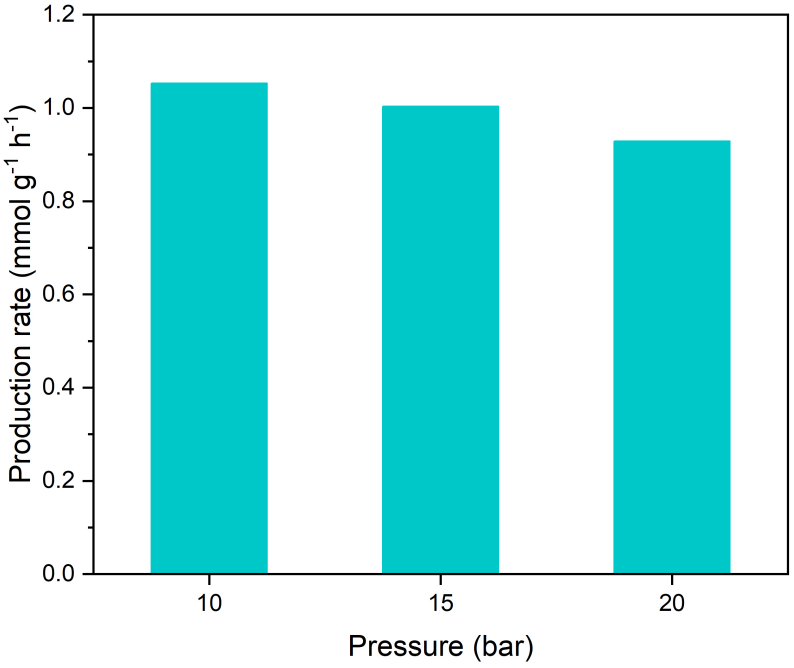

Figure S16. Study of the influence of the operating pressure on the catalytic activity of K-promoted Ru(3)/CeO_2 catalyst for the thermocatalytic NH_3 synthesis. Reaction conditions: $H_2/N_2 = 3$, GHSV = 20,000 mL g^{-1} h^{-1}, 400 °C.

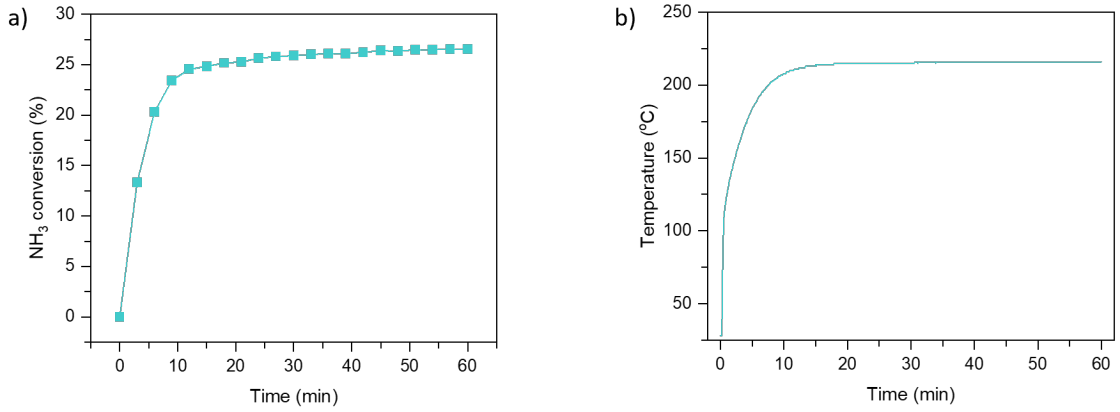

Figure S17. a) NH_3 conversion of K-promoted Ru(3)/CeO_2 catalyst and b) temperature profile under photo-thermal conditions. Reaction conditions: GHSV = 20,000 mL g^{-1} h^{-1}, light intensity 3.3 Wcm^{-2}.

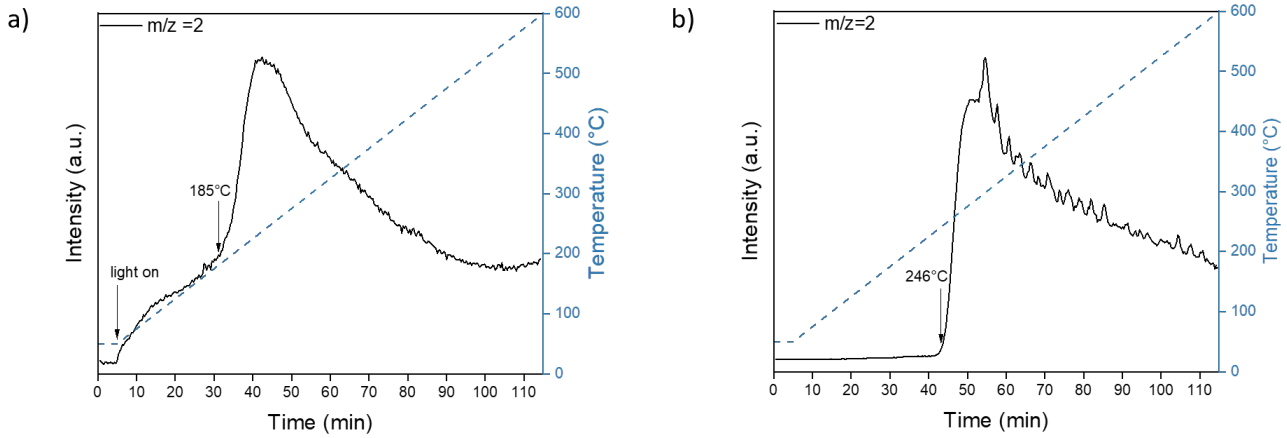

Figure S18. NH_3-TPD of K-promoted Ru(3)/CeO_2 catalyst monitoring the mass of hydrogen in the a) presence and b) absence of light.

Table S4. Summary of the state-of-the-art catalysts for thermal and photo-thermal NH_3 decomposition.

Catalyst	Metal Loading (wt.%)	Conditions	Conversion (%)	H_2 formation rate (mmol g_{Ru}^{-1} h^{-1})	Reference
Ru/SiO_2	10.0	30,000 mL g^{-1} h^{-1} 450 °C	35	6840	[9]
Ru/MCM-41	5.0	30,000 mL g^{-1} h^{-1} 450 °C	42	17040	[9]
Ru/AC	4.8	30,000 mL g^{-1} h^{-1} 450 °C	29	12000	[10]
Ru/CNFs	3.2	6,500 mL g^{-1} h^{-1} 500 °C	99	12360	[11]
Ru/Al_2O_3	5.0	150,000 mL g^{-1} h^{-1} 500 °C	11	21600	[12]
Ru/MgO	4.8	60,000 mL g^{-1} h^{-1} 400 °C	22	18000	[13]
Ru(4)@HTC_2h	5.0	20,000 mL g^{-1} h^{-1} Xe lamp	23	5585	[14]
Fe@C	42.0	1,000 mL g^{-1} h^{-1} Xe lamp	55	694	[15]
Fe@C	42.0	20,000 mL g^{-1} h^{-1} Xe lamp	25	290	[15]
$Ru(3)/CeO_2$	3.4	20,000 mL g^{-1} h^{-1} Xe lamp	27	21867	***This work***

References

1. Peng, Y.; Melillo, A.; Shi, R.; Forneli, A.; Franconetti, A.; Albero, J.; García, H. Light-Assistance in Nitrogen Fixation to Ammonia by Highly Dispersed Cs-Promoted Ru Clusters Supported on ZrO2. *Applied Catalysis B: Environmental* **2023**, *339*, 123143, doi:10.1016/j.apcatb.2023.123143.
2. Peng, Y.; Albero, J.; Franconetti, A.; Concepción, P.; García, H. Visible and NIR Light Assistance of the N2Reduction to NH3Catalyzed by Cs-Promoted Ru Nanoparticles Supported on Strontium Titanate. *ACS Catalysis* **2022**, *12*, 4938–4946, doi:10.1021/acscatal.2c00509.
3. Li, X.; Zhang, X.; Everitt, H.O.; Liu, J. Light-Induced Thermal Gradients in Ruthenium Catalysts Significantly Enhance Ammonia Production. *Nano Letters* **2019**, *19*, 1706–1711, doi:10.1021/acs.nanolett.8b04706.
4. Yi Yang, Pei Wang, Xiaohu Zhang, Shengyao Wang, Xing Ding, Hongshan Ma, HeWang, Yuanzhi Li, Bo Jiang, Hui Song, Xiao Hai, Yue Lu, Hao Chen, and J.Y. Regulating the Scaling Relations in Ammonia Synthesis through a Light-Driven Bendable Seesaw Effect on Tailored Iron Catalyst. *Angewandte Chemie* **2024**, doi:10.1016/0009-2509(62)87032-8.
5. Sousa, A.; Rendon Patino, A.; Garzon Tovar, L.; Mateo, D.; Gascon, J.; Bavykina, A. Ammonia Decomposition via MOF-Derived Photothermal Catalysts. *ChemSusChem* **2024**, *202401896*, 1–5, doi:10.1002/cssc.202401896.
6. Bian, X.; Zhao, Y.; Waterhouse, G.I.N.; Miao, Y.; Zhou, C.; Wu, L.; Zhang, T. Quantifying the Contribution of Hot Electrons in Photothermal Catalysis: A Case Study of Ammonia Synthesis over Carbon-supported Ru Catalyst. *Angew Chem Int Ed* **2023**, *62*, e202304452, doi:10.1002/anie.202304452.
7. Mao, C.; Wang, J.; Zou, Y.; Shi, Y.; Viasus, C.J.; Loh, J.Y.Y.; Xia, M.; Ji, S.; Li, M.; Shang, H.; et al. Photochemical Acceleration of Ammonia Production by Pt_1 -Pt_n -TiN Reduction and N_2 Activation. *J. Am. Chem. Soc.* **2023**, *145*, 13134–13146, doi:10.1021/jacs.3c01947.
8. Zhang, T.; Zhang, X.; Chang, F. Synergistic Photothermal Acceleration of Ammonia Synthesis Using Defective TiO_2 Supported Ru Catalysts. *Ind. Eng. Chem. Res.* **2025**, *64*, 14879–14887, doi:10.1021/acs.iecr.5c02153.
9. Li, X.K.; Ji, W.J.; Zhao, J.; Wang, S.J.; Au, C.T. Ammonia Decomposition over Ru and Ni Catalysts Supported on Fumed SiO 2, MCM-41, and SBA-15. *Journal of Catalysis* **2005**, *236*, 181–189, doi:10.1016/j.jcat.2005.09.030.
10. Yin, S.F.; Xu, B.Q.; Zhu, W.X.; Ng, C.F.; Zhou, X.P.; Au, C.T. Carbon Nanotubes-Supported Ru Catalyst for the Generation of CO x-Free Hydrogen from Ammonia. *Catalysis Today* **2004**, *93–95*, 27–38, doi:10.1016/j.cattod.2004.05.011.
11. Duan, X.; Zhou, J.; Qian, G.; Li, P.; Zhou, X.; Chen, D. Carbon Nanofiber-Supported Ru Catalysts for Hydrogen Evolution by Ammonia Decomposition. *Cuihua Xuebao/Chinese Journal of Catalysis* **2010**, *31*, 979–986, doi:10.1016/s1872-2067(10)60097-6.
12. Yin, S.F.; Zhang, Q.H.; Xu, B.Q.; Zhu, W.X.; Ng, C.F.; Au, C.T. Investigation on the Catalysis of COx-Free Hydrogen Generation from Ammonia. *Journal of Catalysis* **2004**, *224*, 384–396, doi:10.1016/j.jcat.2004.03.008.
13. Yin, S.F.; Xu, B.Q.; Wang, S.J.; Ng, C.F.; Au, C.T. Magnesia-Carbon Nanotubes (MgO-CNTs) Nanocomposite: Novel Support of Ru Catalyst for the Generation of COx-Free Hydrogen from Ammonia. *Catalysis Letters* **2004**, *96*, 113–116, doi:10.1023/B:CATL.0000030107.64702.74.
14. Rendon-Patiño, A.; Mateo, D.; Duran-Uribe, S.; Sepulveda-Escribano, A.; Gascon, J.; Ramos-Fernandez, E. V. Ruthenium Nanoparticles within Carbon Spheres for Efficient Ammonia Decomposition. *ChemCatChem* **2024**, *202400878*, doi:10.1002/cctc.202400878.
15. Sousa, A.; Mateo, D.; Garzon-Tovar, L.; Brennan, K.; Rendón-Patiño, A.; Morlanés, N.; Wang, X.; Navarro, J.C.; Ruiz-Martinez, J.; García-Melchor, M.; et al. Unlocking Low-Temperature Ammonia Decomposition via an Iron Metal–Organic Framework-Derived Catalyst Under Photo-Thermal Conditions. *Small* **2025**, *2411468*, 1–9, doi:10.1002/smll.202411468.